Forward Projected Background Oriented Schlieren for Study of Sparks in Internal Combustion Engines

Saraschandran Kottakalam[1,*], Gregor Rottenkolber[1], Christian Trapp[2]

1: Faculty of Mobility and Technology, Esslingen University of Applied Sciences, Germany
2: Professor für Fahrzeugantriebe, University of the Bundeswehr Münich, Germany
*Corresponding author: saraschandran.kottakalam@hs-esslingen.de

Keywords: BOS, Sparks, Micro calorimetry, FPBOS.

ABSTRACT

The use of renewable fuels, such as hydrogen, in internal combustion engines requires novel combustion strategies that require a deep understanding of their ignition phenomena. This leads to the need for improved or new measurement techniques that can provide further insight into these phenomena. As part of a study to better understand the ignition phenomenon, this paper presents a modified Background Oriented Schieren method developed to study the heat transfer from sparks generated by spark plugs. This new method is called Forward Projected Background Oriented Schlieren or FPBOS, and this is the first time such a method has been introduced to the best of the authors' knowledge. FPBOS provides a flexible and more powerful alternative to other BOS techniques, especially for use in micro-calorimetry applications. It can be used similarly to any other BOS method and with different correlation algorithms. This study presents a detailed account of this technique and its use to obtain high resolution, high speed visualisation of the heat transfer from the spark to the environment and the interaction of the spark with the flow field.

1. Introduction

Due to the recent push to switch to renewable fuels, new combustion strategies and concepts need to be developed that can give rise to internal combustion engines (ICEs) that can compete with the existing engines running on petrol or diesel. Among the renewable fuels, hydrogen is in the focus of immediate research because it is the simplest e-fuel and is carbon-free. The development and optimization of combustion concepts (such as hydrogen combustion) and new components (such as prechamber spark plugs) require deep understanding of the ignition phenomenon. However, there is still a lack of knowledge about the modelling of sparks in terms of heat transfer, ignition location and flame kernel formation for classical combustion concepts using gasoline.

The energy transfer from the plasma to the surrounding charge gas has a significant impact on the ignition process and it is therefore crucial. This is because the plasma consists entirely of

ions and hardly any combustion reaction can occur inside the plasma channel. However, the volume surrounding the plasma is heated by it and creates conditions ideal for combustion reactions. Therefore, this research focuses on a new experimental technique (Forward Projected Background Oriented Schlieren, FPBOS), which enables high resolution, high-speed visualisation and even quantification of high density gradients and temperatures in small observation fields.

2. Measurement principle - Background Oriented Schlieren (BOS)

In order to visualise the heat transfer from the plasma to the surrounding, Background Oriented Schlieren (BOS) was adopted since this technique makes it possible to visualise the density change in the medium (caused by the heat transfer from plasma in this case). BOS works on the principle that refractive index of a medium is dependent on the density of the medium as stated by the Gladstone-Dale equation. As a consequence, light rays passing through this density gradient would be refracted. A schematic representation of BOS technique and the refraction of light rays through by the density gradient is shown in Figure 1.

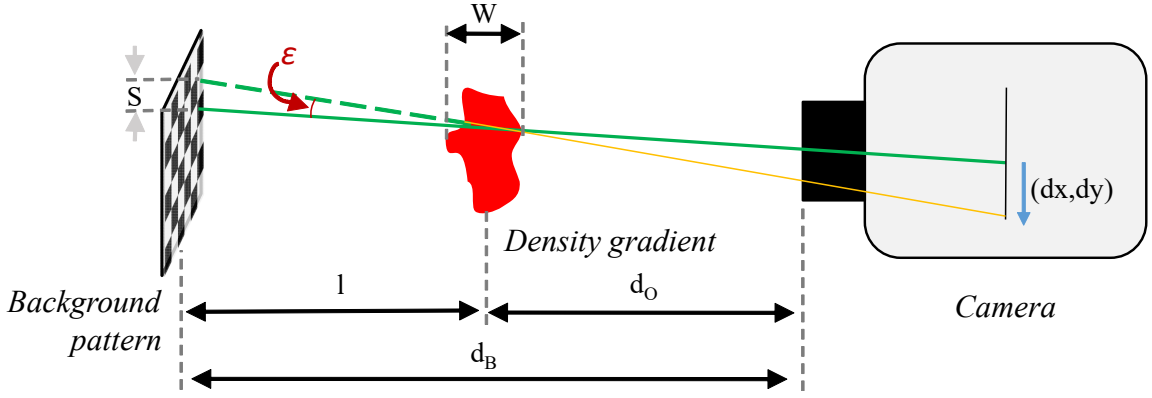

Figure 1. Schematic of BOS with the background, density gradient and the camera

In order to visualise and quantify the density gradient in a medium, BOS utilizes algorithms (Digital image correlation (DIC), Fast Checkerboard Demodulation (FCD), Optical flow) which can compare two images of a background pattern taken by a camera; one with and one without the influence of the density gradient. These algorithms are able to calculate the displacements in this background caused by refraction. Since the angle of refraction is proportional to the change in refractive index, a quantitative information about the density gradients can be obtained from the output of these algorithms taking into account the geometric setup of the measurement (Raffel, 2015). The apparent shift of the background pattern due to the change in refractive index is provided by equation 1 (Van Hinsberg & Rösgen, 2014)(Kaneko et al., 2021)(Dalziel et al., 2000).

$$S = \frac{1}{C} W(W + 2l) \frac{1}{n_0} \nabla n \tag{1}$$

Here, n_0 is the reference refractive index, l is the distance between the density gradient and the background, W is the thickness of the density gradient and S is the shift observed in the plane of the background derived from the output of the correlation algorithms. C is a constant dependent on the thickness of the density gradient and defined according to equation 2.

$$C = \frac{2}{1 + \frac{W}{2l}} \tag{2}$$

Further, the refractive index is related to the density of the medium, the refractive index n and the Gladstone-Dale constant K for a given wavelength of light according to the Gladstone-Dale relation as in equation 3.

$$\rho = \frac{n - 1}{K} \tag{3}$$

However, it has to be noted that the Gladstone-Dale expression given above is not valid for the spark itself. This is because at very high temperatures (T > 2000 K), the chemical composition of the gas changes due to molecular dissociation and atomic ionization processes which can affect refractive index (Stoller et al., 2014). However, Michalski et al. (2018) explains that the influence of the charged particles of plasma on the refractive index is negligible. Nevertheless, this work does not focus on measuring plasma temperatures but on the temperature of the plasma surroundings.

On substituting equation 3 in equation 1 obtains equation 4. This equation remains valid even when the density gradient thickness (W) is not negligible in comparison to the distance between the density gradient and the background pattern (l), which is described as Near-field BOS or NF-BOS.

$$S = \frac{1}{C} W(W + 2l) \frac{K}{K\rho_0 + 1} \nabla\rho \tag{4}$$

Here, ρ_0 is the reference density. Rearranging and differentiating the equation on both sides forms the Poisson's equation 5 which can be solved to obtain the density field.

$$\nabla^2\rho = \frac{C(K\rho_0 + 1)}{W(W + 2l)K} \nabla \cdot S \tag{5}$$

However, equations 5 and 2 are given for conditions when either the thickness of the density gradient along the entire view-field (W(x,y)) is known (Van Hinsberg & Rösgen, 2014) or when the thickness of the density gradient remains constant throughout the view-field (Kaneko et al., 2021). This is not the case for the experiments performed as part of this study. Obtaining the thickness of the density gradient generated by the spark would be difficult due to the complex

shapes generated which depends on the electrode geometry and the flow conditions. Therefore, a calibration term was introduced to get the 'effective thickness' of the density gradient which can be obtained using a density gradient with similar cylindrical shape.

From the density field, assuming the pressure to be constant, temperature can be calculated using the ideal gas equation 6, where T represents the temperature in Kelvin, p represents the pressure, ρ is the density and R represents the gas constant.

$$T = \frac{p}{\rho R} \tag{6}$$

Due to the high temperature of approx. 4000 K (Michler et al., 2020) in the plasma channel, which is approximately 0.3 mm in diameter, a high-density gradient is generated in a very small field of observation. Standard BOS techniques face difficulties in addressing these conditions. As a result, a new variation of BOS named Forward Projected Background Oriented Schlieren (FPBOS) was developed which offers several advantages over the standard BOS techniques for this particular application. An overview of the method was presented in Kottakalam et al. (2023) for high-speed visualisation of the density gradients generated by the sparks produced by an induction coil ignition system used in series automotive production. This technique will be further explained in 3.3.

3. Experimental setup

The experimental setup is divided into four sections, each of which is explained in detail below.

3.1. Wind tunnel test-bed

The wind tunnel spark test-bed for testing sparks is designed for observing sparks under engine conditions. It enables the testing of sparks at pressures of up to 40 bar and a flow velocity of up to 40 m/s with an option to heat the flowing medium up to 180 °C. The tests are performed with a non-combustible medium, either nitrogen or air. The test bed shown in Figure 2 provides optical access to the sparks through two glass windows located on either side of the main chamber. The spark plug (series J-gap spark plug with 0.7 mm electrode gap) orientation can also be changed according to the requirements by a modifiable flange. A standard automotive induction coil ignition system with 1.2 ms dwell time was used for the experiments.

The spark test-bed allows both electrical and optical observation of sparks. The secondary electrical properties are observed with Tektronix P6015A probe and FOS OCS 1000 current probe. The readings from these probes are then recorded by using an oscilloscope (Yokogawa DLM4038).

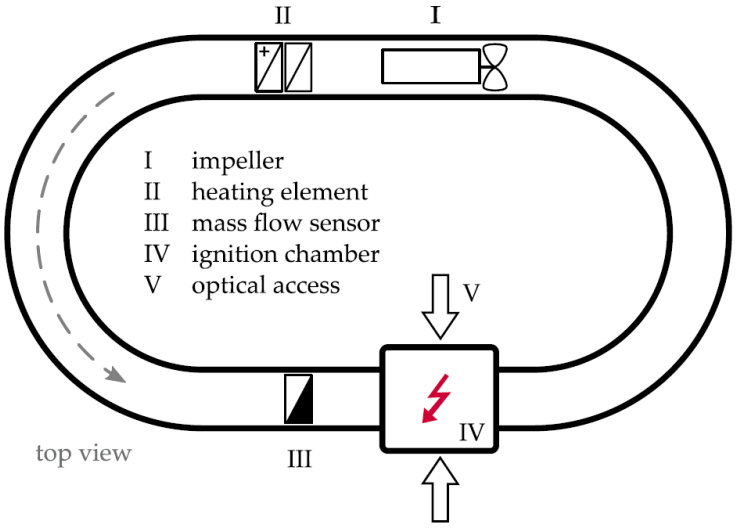

Figure 2. Schematic of the wind canal testbed (Wörner & Rottenkolber, 2021)

3.2. High speed camera setup

The optical observations are carried out by high-speed camera, Photron FASTCAM SA-X2, up to a capturing frequency of 500 kHz. This camera is capable of detecting emissions in the 400-1000 nm wavelength range. Based on the objective of the experiment, the camera is coupled with either a Tokina AF 100mm f/2,8 Macro AT-X or MVL12X12Z Zoom-lens from Thorlabs which allows a high spatial resolution visualisation of the electrode gap of the spark plug.

3.3. Forward Projected Background Oriented Schlieren (FPBOS)

In this technique, instead of a physical background pattern, a projector is used to project a pattern directly onto the camera's focus plane. The schematic of the setup is shown in the Figure 3.

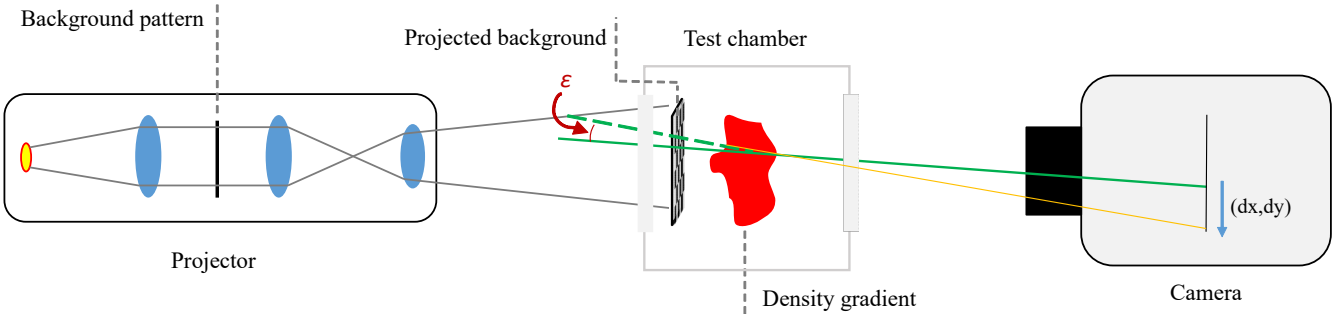

Figure 3. Schematic of Forward Projected Background Oriented Schlieren (FPBOS)

The projected pattern could be any of the patterns typically used for BOS measurements like a

periodic pattern (eg. checkerboard) or a random dot pattern. Key advantages over the standard BOS techniques:

- The pattern size can be varied 'on-the-fly' by adjusting the optical setup.
- The pattern can be projected onto any plane required (subject to the limitations of the optics) without influencing the flow field.

These features makes it especially suited for observing sparks due to the reasons explained below:

- Since the tests are performed in a pressurized chamber with flow, it is not possible to have a physical pattern inside. However, the projector makes it possible for it to be projected anywhere required. This allows the sensitivity of the setup to be adjusted which is required when different measurement conditions (eg. pressure) are used.
- The field of observation (approx. 10 x 10 mm) and the volume of density gradient is very small which requires the pattern size to be small for high-resolution visualisation. This increases the sensitivity of the setup.
- The high temperatures (approx. 4000 K (Michler et al., 2020)) inside the plasma channel and the small volume involved, coupled with the extremely small time scales (entire spark event takes place in less than 1.5 ms) lead to the generation of extremely high-density gradients. This means the sensitivity of the set up must be sufficiently low for the algorithm to detect the distorted pattern. This is necessary to obtain quantitative information.

These features enable the possibility to have a setup with high spatial resolution by using really small patterns (limit being the aliasing caused by the spatial resolution of the sensor in the camera). This in combination with a high zoom lens would result in displacement vector field with exceptional spatial resolution. Along with the ability to bring the sensitivity of the setup low (by reducing distance l), FPBOS forms an ideal setup to observe density gradients generated by the sparks under engine conditions.

3.3.1. FPBOS setup

The FPBOS setup used for this setup has three main sections. Namely the projector, the light source and the background pattern.

- The projector comprises two collimating achromatic lenses and a focusing achromat, all of which have a diameter of 40 mm. The collimating achromats have a focus length of 160 mm, while the third focusing lens has a focus length of 120 mm. The collimating lenses are fixed in position relative to one another, while the focus lens can be moved for focusing purposes.

- The background pattern is printed on a transparent foil and positioned between the two collimating lenses. The pattern employed for these measurements is a simple checkerboard pattern with a checker size of 0.25 mm. The limiting factor in this case is the quality of the print that can be obtained from the printer. Nevertheless, the size can be modified in real time by adjusting the distance between the focusing lens and the collimating lens. Furthermore, the ability to control the location and plane of focus of the pattern allows for the sensitivity of the setup to be varied, thereby enhancing the setup's flexibility.
- The light source is a Nichia NV4L144ART SMD-LED, which emits light in the visible spectrum and illuminates the background pattern.

3.4. Matlab implementation

The operations for displacement vector calculation and the subsequent density calculations are performed by Matlab scripts. The algorithm used for this research is Fast Checkerboard Demodulation (FCD), introduced by (Wildeman, 2018) owing to its advantages in comparison to methods like Digital Image Correlation (DIC), that was further investigated by (Shimazaki et al., 2022). This algorithm obtains the displacement field by quantifying the deformation of a periodic background pattern (checkerboard in this case) when observed through a density gradient.

The script used for the calculations is a modified version of FCD algorithm made available by Wildeman (2018). The displacement vectors obtained by this algorithm is then used to solve the Poisson's equation 5 by central difference scheme until a tolerance of 1e-10 is reached. A combination of Dirichlet (along the vertical edges) and Neumann (along the horizontal edges) conditions were used as boundary conditions.

4. Results

The results obtained using the setup explained in section 3 is presented and discussed in this section.

4.1. Temperature field from sparks

In order to measure the temperature from a displacement field, it is essential to calibrate the setup. This is due to the inherent uncertainties in the measured geometrical parameters, as previously discussed in section 2. From experiments, it was observed that the density gradient thickness has a significant influence on the temperature calculations from BOS. As previously discussed, equation 5 utilizes a matrix of density gradient thickness values for the entire view field (Van Hinsberg & Rösgen, 2014). However, the thickness of the density gradient generated by sparks is challenging

to ascertain due to the intricate shapes involved. Consequently, the methodology employed in this study entails the estimation of an 'effective thickness' based on the measured thickness of the density gradient.

4.1.1. Calibration

A butane gas jet lighter was used for the calibration. The choice was made based on the similarity in the shape of the density gradients even though it is thicker than that generated by the spark. From temperature field measurements shown in figure 4, the gradient thickness was measured from the plot to be 3.5 mm and a correction factor was used to obtain the 'effective gradient thickness', $W_{eff} = W \times Correction factor$. W_{eff} is then used to calculate the correction factor C in equation 2 and subsequently solve equation 5. Which are now defined as equations 7 and 8.

$$C = \frac{2}{1 + \frac{W_{eff}}{2l}} \tag{7}$$

$$\nabla^2 \rho = \frac{C(K\rho_0 + 1)}{W_{eff}(W_{eff} + 2l)K} \nabla \cdot S \tag{8}$$

The experiments were conducted under ambient temperature (300 K) and pressure conditions (1 bar) with air as the medium. The geometric parameters of the measurement setup are mentioned in table 1. The resultant view field is 7.3 mm x 14.4 mm with a spacial resolution of 0.0267 mm per pixel.

Table 1. Geometric parameters for the experiment

d_O	d_B	l
160 mm	150 mm	-10 mm

In order to facilitate calibration, the temperatures at different points in the view field were measured by means of a temperature probe. The temperature was then calculated for various calibration factors by solving the Poisson's equation 5 and compared to the measured temperature. For a calibration factor value of 0.07, the calculated temperatures were similar to the measured temperatures. This was then used for the temperature calculation and the resulting temperature field is as shown in figure 4.

Table 2 shows the comparison of the temperatures measured along different locations in the view-field to the measured temperature using temperature sensors. In part, the observed deviations can be attributed to the strong temperature gradients present within the flame and the precision with which the temperature probe could be positioned.

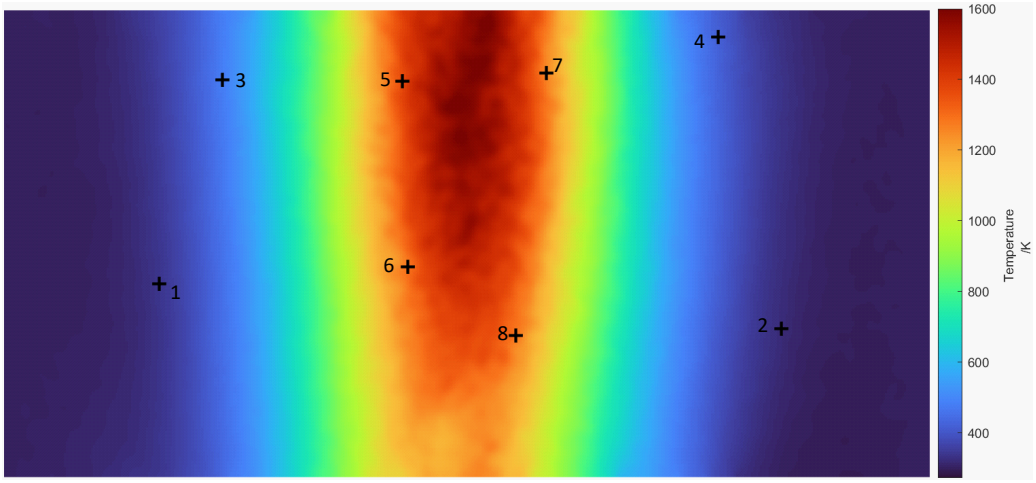

Figure 4. Temperature field calculated for the gas jet lighter after calibration with temperature measurement locations 1-8 shown

Table 2. Comparison - calculated and measured temperature

Location	Measured temperature in K	Calculated temperature in K
1	314	337
2	393	322
3	493	475
4	673	423
5	1153	1366
6	1333	1285
7	1488	1261
8	1498	1293

4.1.2. Spark - temperature field

Under the same conditions mentioned in section 4.1.1, FPBOS measurements were carried out with the density gradients generated by a spark at no-flow conditions at a capturing frequency of 50 kHz. The equipment used for this was described in section 3. The generated spark is sustained between the electrodes for a duration of approximately 1.7 ms.

The calibration factor of 0.07 obtained from the section 4.1.1 and the measured thickness of the density gradient immediately following breakdown (0.6 mm) were employed to determine the 'effective thickness' of the density gradient. This was then utilised to calculate the temperature field for the spark. Figure 5 shows the temperature field calculated at a time of 0.1 ms after the breakdown.

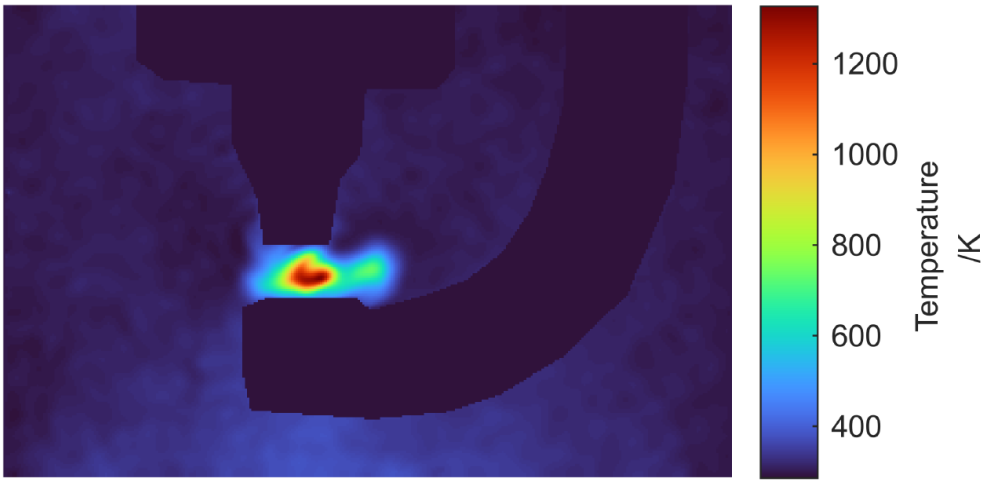

Figure 5. Temperature field for the spark at 0.1 ms after the breakdown

Initial observations of the temperature field shows that the calculations seem to predict the physical effects of the spark qualitatively. The temperature is the highest in the middle and gets colder near the electrodes. This could be due to the heat being transferred from the spark to the electrodes. Another contributing factor to this is the applied boundary conditions. As explained in a previous section, the boundary conditions are along the edges of the view-field and the noise in the region of the electrodes are masked. This means that no boundary conditions are applied to the spark-electrode boundary. However, applying Neuman boundary conditions here could not be the best solution since the temperature difference in the spark-electrode interface is expected to be significant.

Temperature field calculations for various time steps throughout the discharge is shown in figure 6. On inspection, it was seen that once again the results follow the expectations. The temperatures remain the highest in the middle of the electrodes with highest temperatures reaching 4000 K in certain time-steps and getting colder near the electrodes. This trend is more pronounced as the discharge progresses further which is also expected due to the heat loss through conduction through the electrodes. It can be observed that the temperature rises initially as the discharge continues, then declines as the energy in the coil diminishes due to the discharge and also due to the heat conducted through the electrodes. Finally, the temperature falls significantly as the discharge comes to an end (after 1.7 ms). This observed trend over time is analogous to the one previously documented by Kim et al. (2018) for the rotational temperature in plasma.

As previously stated, the outcomes are significantly influenced by the thickness of the density gradient. For each time step depicted in the figure 6, a constant density gradient thickness of 0.6 mm was employed, which was measured from FPBOS results immediately following the breakdown. However, this assumption neglects the impact of the surrounding heated gas at lower tempera-

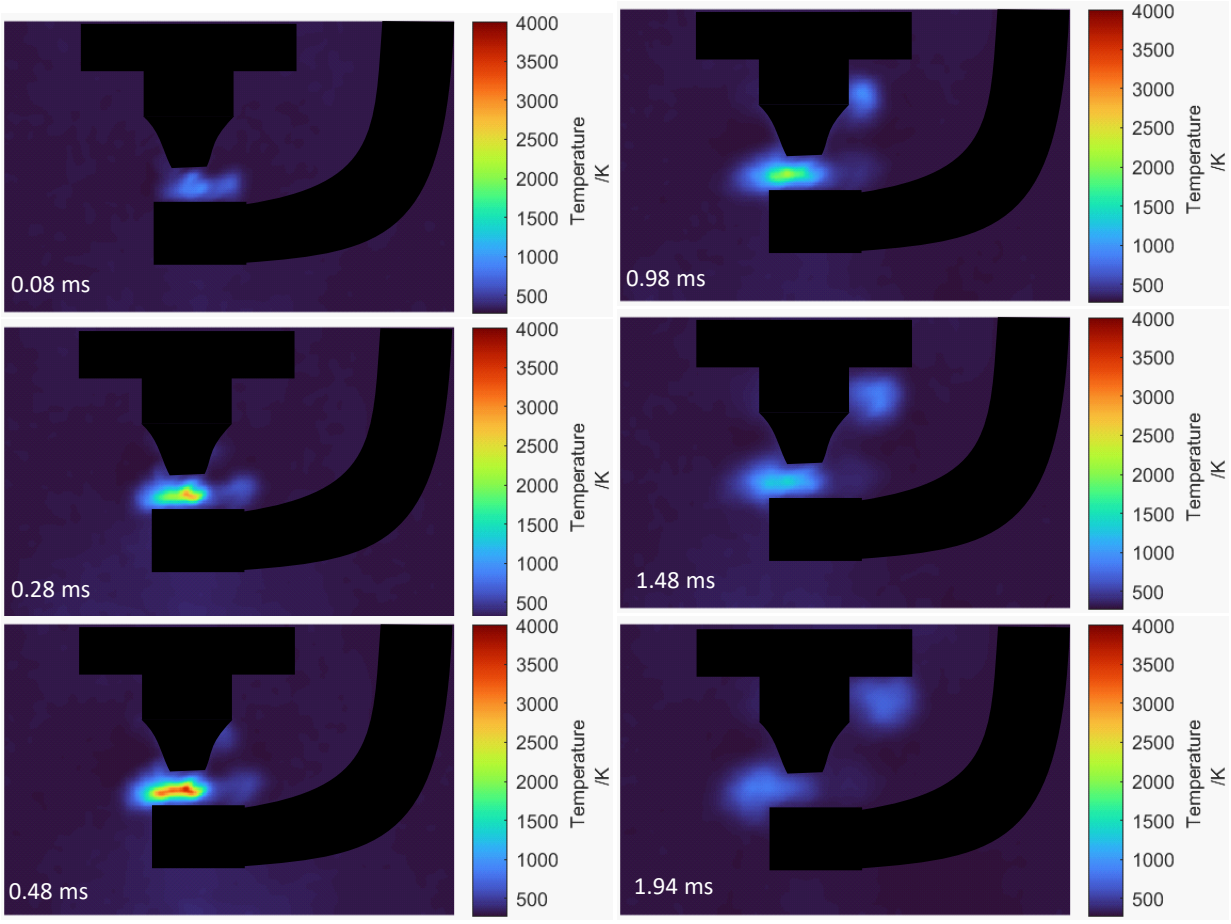

Figure 6. Temperature field at different time-steps (Time after breakdown shown in respective frames)

tures. This could potentially lead to an overestimation of the actual temperature in the calculations. This is because, the longer the discharge occurs, the thicker the density gradient becomes. It is of the utmost importance to bear this in mind in order to prevent errors in calculations. Nevertheless, this calibration provides a temperature field that is not significantly different from the values reported in open literature (Michler et al., 2020) (Michalski et al., 2018) (Kim et al., 2018).

4.2. Flow field - spark interaction

Figure 7 shows both the visible spark as well as the density gradient generated by the sparks formed under the same conditions (different spark events). They are captured at 50 kHz. All frames depict the location of the central and the mass electrodes of the J-gap spark-plug used for the study. The initial set of images show the spark captured 0.02 ms after the breakdown, followed by subsequent images at 0.04 ms intervals, demonstrating the spark's development. The images were captured by using Zoom-lens and the geometric conditions for the FPBOS measurements are mentioned in the table 3.

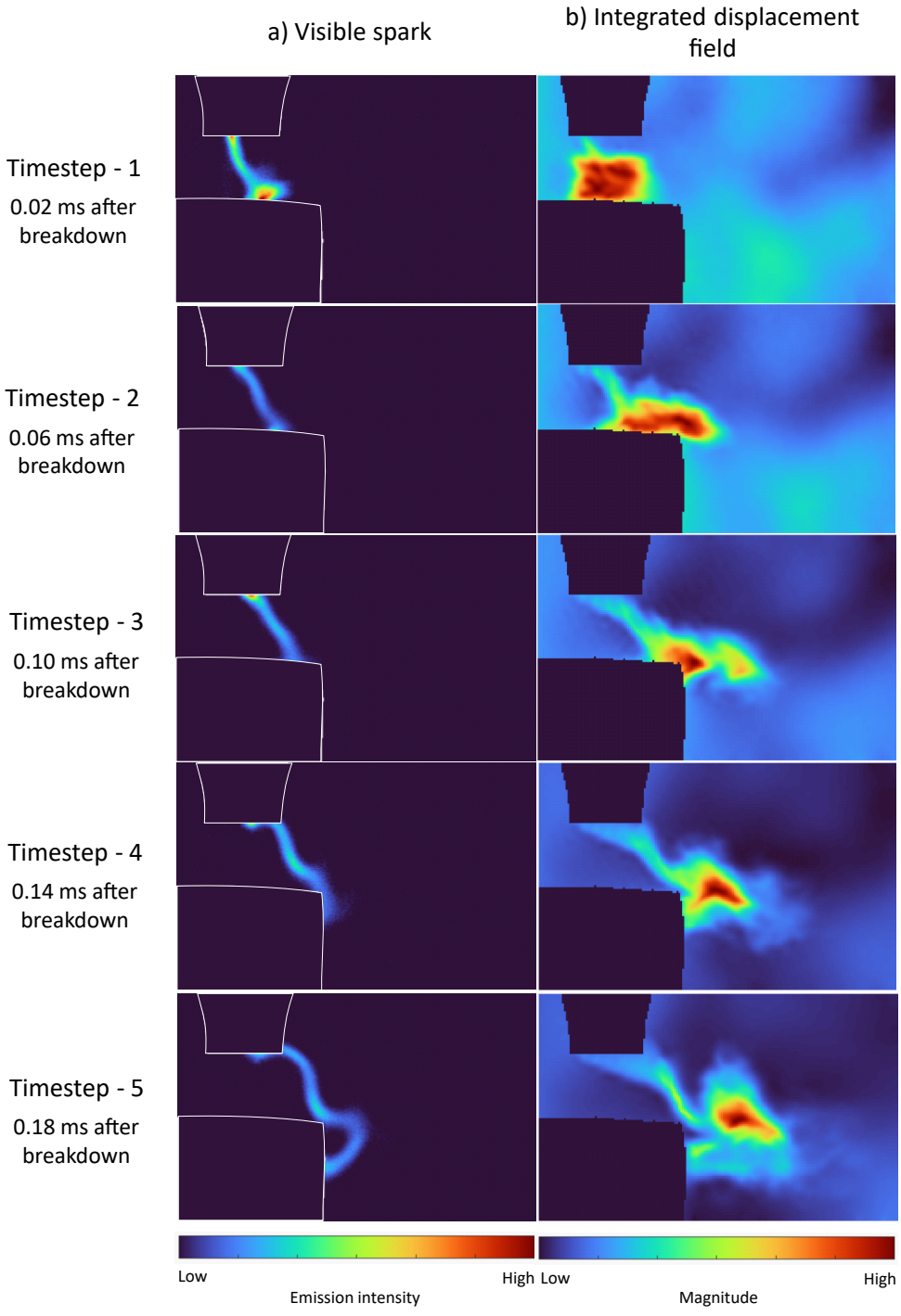

Figure 7. Visible plasma channel and the density gradients generated at 11 bar (abs. pressure) and 10 m/s flow from the left

Table 3. Geometric parameters for the FPBOS measurement

d_O	d_B	l
167 mm	168 mm	1 mm

The images of the visible spark in the left column (a) are post processed with false colour applied for higher contrast and clear depiction of the plasma channel. The images depicted in the right column (b) shows the area (2D information) heated by the spark/plasma channel. For better visualisation, the displacement vector field obtained from the FCD algorithm is integrated and depicted.

As mentioned in the previous section, the temperature calculation is based on the geometric parameters of the setup and is extremely sensitive to the thickness of the density gradient. The presence of components like the electrodes in the field of flow creates a complicated flow characteristic inside the test bed. This makes it extremely difficult to obtain the location of the density gradient along the line of sight at each time-step which is required for temperature calculation as per equation 5. The calibration technique mentioned in section 4.1 also cannot be adopted since the flow generates complicated density gradient shape/form that is not comparable to the shape of the gas-jet lighter. However, FPBOS can still be used to obtain valuable insight about the flow-spark interactions as well as information about the flow field around the spark plug.

On comparing the visible sparks to the volume heated by the plasma made visible through the FPBOS measurement technique, it can be seen that the excited plasma is only a small volume in comparison to the heated volume. This is a significant factor to consider, as the heated volume exerts a considerable influence on the initiation of ignition, which in turn has a profound impact on the initial stages of combustion.

Another valuable information that can be derived from this experiment is an understanding of the interaction between the plasma and the flow field. It can be seen that the plasma is slower in comparison to the flow. However, the flow field conducts the heat from the plasma channel and as a result, the heated region travels faster than the plasma. This is a valuable insight, as it could prove instrumental in achieving consistent and predictable ignition. The greater the distance between the first flame kernel and the walls, the lower the probability of the flame being extinguished. This is of great significance, for instance, in the context of prechamber design.

FPBOS technique also makes it possible to observe additional phenomena that happens during the spark development. An example of this is the heated area that seems to be being reflected from the mass electrode surface as seen in images 1b and 2b immediately following the breakdown. This phenomenon is not detectable with visible spark observations. However, this creates a volume of heated medium that is carried away by the flow even-though the plasma channel is still between the electrodes. Heat transfer visualisation also provides the possibility to understand the flow

field near the spark plug better like the location where the heated volume is concentrated and the stagnation zones around the spark plug. This is always critical for the initial flame kernel formation and propagation (Herweg, 1992).

5. Conclusions

From the results, it can be seen that this new measurement technique, Forward Projected Background Oriented Schlieren (FPBOS), provides new information about sparks which helps in the design of new combustion concepts and also components like prechamber spark plugs.

Key findings from the use of FPBOS observations for the observation of sparks include:

1. Quantitative temperature field created by spark in a no-flow condition was obtained.
2. Spark heated flowing medium observed with high spatial resolution enabling better understanding of heat transfer from spark as well as flow around spark plugs.

These observations establishes that FPBOS technique is extremely flexible and can be easily adapted for a plethora of use cases with on-the-fly adjustment capabilities, which traditional BOS techniques tend to lack. It enables sensitivity and resolution adjustment according to immediate requirements of the test conditions. This is key for high temporal and spatial resolution density gradient visualisation along with the possibility to measure high temporal resolution temperature fields with acceptable spatial resolution. These add to the information that can be obtained regarding the spark ignition which is critical to drive innovation forward.

6. Outlook

Measurement situations where the density gradient is not in a single plane (eg. due to non-steadily flowing medium) can have a significant influence on the signal strength and, subsequently, the calculated temperature fields. This is especially true when the distance between the spark and the background becomes very small (i.e. l approaches zero). Furthermore, as previously stated, the thickness of the density gradient exerts a profound influence on the temperature calculations. This renders the calculation of the temperature field for complex geometries challenging. Such situations needs to be further investigated.

Acknowledgements

This work was funded by dtec.bw. dtec.bw is funded by the European Union – NextGenerationEU. The authors also gratefully acknowledge the help of colleagues from Esslingen University of Ap-

plied sciences, Mr. Christoph Spang and Mr. Tim Schwellinger.

References

Dalziel, S., Hughes, G., & Sutherland, B. (2000, 01). Whole-field density measurements by 'synthetic schlieren'. *Experiments in Fluids*, *28*, 322-335. doi: 10.1007/s003480050391

Herweg, R. (1992). *Die entflammung brennbarer, turbulenter gemische durch elektrische zündanlagen - bildung von flammenkernen*.

Kaneko, Y., Nishida, H., & Tagawa, Y. (2021, aug). Background-oriented schlieren measurement of near-surface density field in surface dielectric-barrier-discharge. *Measurement Science and Technology*, *32*(12), 125402. doi: 10.1088/1361-6501/ac1ccc

Kim, W., Bae, C., Michler, T., Toedter, O., & Koch, T. (2018, 12). Spatio-temporally resolved emission spectroscopy of inductive spark ignition in atmospheric air condition.. doi: 10.5445/IR/1000088260

Kottakalam, S., Alkezbari, A., Rottenkolber, G., & Trapp, C. (2023). Developing optical measurement techniques for improving ignition simulation models. In *14th International ERCOFTAC Symposium on Engineering Turbulence Modelling and Measurements, Barcelona, Spain*.

Michalski, Q., Benito Parejo, C. J., Claverie, A., Sotton, J., & Bellenoue, M. (2018). An application of speckle-based background oriented schlieren for optical calorimetry. *Experimental Thermal and Fluid Science*, *91*, 470-478. Retrieved from `https://www.sciencedirect.com/science/article/pii/S0894177717302844` doi: https://doi.org/10.1016/j.expthermflusci.2017.09.012

Michler, T., Toedter, O., & Koch, T. (2020). Measurement of temporal and spatial resolved rotational temperature in ignition sparks at atmospheric pressure. *Automotive and Engine Technology*.

Raffel, M. (2015). Background-oriented schlieren (bos) techniques. *Springerlink.com*.

Shimazaki, T., Ichihara, S., & Tagawa, Y. (2022). Background oriented schlieren technique with fast fourier demodulation for measuring large density-gradient fields of fluids. *Experimental Thermal and Fluid Science*, *134*, 110598. Retrieved from `https://www.sciencedirect.com/science/article/pii/S0894177722000036` doi: https://doi.org/10.1016/j.expthermflusci.2022.110598

Stoller, P. C., Panousis, E., Carstensen, J., Doiron, C. B., & Färber, R. (2014, nov). Speckle measurements of density and temperature profiles in a model gas circuit breaker. *Journal of Physics D:*

Applied Physics, *48*(1), 015501. Retrieved from https://dx.doi.org/10.1088/0022-3727/48/1/015501 doi: 10.1088/0022-3727/48/1/015501

Van Hinsberg, N., & Rösgen, T. (2014, 03). Density measurements using near-field background-oriented schlieren. *Experiments in Fluids*, *55*. doi: 10.1007/s00348-014-1720-x

Wildeman, S. (2018). Real-time quantitative schlieren imaging by fast fourier demodulation of a checkered backdrop. *Experiments in Fluids*, *59*. Retrieved from https://doi.org/10.1007/s00348-018-2553-9 doi: 10.1007/s00348-018-2553-9

Wörner, M., & Rottenkolber, G. (2021). Voltage rise anemometry in turbulent flows applied to internal combustion engines. *Experiments in Fluids*, *62*(132). Retrieved from https://link.springer.com/article/10.1007/s00348-021-03226-3 doi: https://doi.org/10.1007/s00348-021-03226-3